Limiting factors to the OCT axial resolution for *in-vivo* imaging of human and rodent retina in the 1060nm wavelength range

Sepideh Hariri[1], Alireza A. Moayed[1], Aphrodite Dracopoulos[2], Chulho Hyun[1], Shelley Boyd[2] and Kostadinka Bizheva[1]*

[1]*Department of Physics and Astronomy University of Waterloo, Waterloo, ON, N2L 3G1, Canada*
[2]*Department of Ophthalmology and Vision Science, St. Michaels Hospital and University of Toronto, Toronto, ON, M5B 1W8, Canada*
**kbizheva@uwaterloo.ca*

Abstract: A computational model was developed to evaluate the limitations to the highest axial resolution, achievable with ultrahigh resolution optical coherence tomography (UHROCT) in the 1060nm wavelength region for *in-vivo* imaging of the human and rodent retina. The model considers parameters such as the wavelength dependent water absorption, the average length of the human and rodent eyes, and the power limitations for the imaging beam as defined in the ANSI standard. A custom-built light source with re-shaped spectrum was used to verify experimentally the results from the computational model. Axial OCT resolution of 4.2μm and 7.7μm was measured from a mirror reflection with the custom light source by propagating the imaging beam through water cells with 5mm and 25mm thickness, corresponding to the average axial length of the rodent and human eye respectively. Assuming an average refractive index of 1.38 for retinal tissue, the expected axial OCT resolution in the rodent and human retina is 3μm and 5.7μm respectively. Retinal tomograms acquired *in-vivo* from the rat eye with the modified light source show clear visualization of all intraretinal layers, as well as a network of capillaries (~10μm in diameter) in the inner- and outer plexiform layers of the retina.

OCIS codes: (170.4500) Optical coherence tomography; (170.4470) Ophthalmology; (170.3880) Medical and biological imaging.

References and links

1. B. Považay, K. Bizheva, B. Hermann, A. Unterhuber, H. Sattmann, A. F. Fercher, W. Drexler, C. Schubert, P. K. Ahnelt, M. Mei, R. Holzwarth, W. J. Wadsworth, J. C. Knight, and P. S. Russell, "Enhanced visualization of choroidal vessels using ultrahigh resolution ophthalmic OCT at 1050 nm," Opt. Express **11**(17), 1980–1986 (2003).
2. A. Unterhuber, B. Povazay, B. Hermann, H. Sattmann, A. Chavez-Pirson, and W. Drexler, "In vivo retinal optical coherence tomography at 1040 nm - enhanced penetration into the choroid," Opt. Express **13**(9), 3252–3258 (2005).
3. E. C. W. Lee, J. F. de Boer, M. Mujat, H. Lim, and S. H. Yun, "In vivo optical frequency domain imaging of human retina and choroid," Opt. Express **14**(10), 4403–4411 (2006).
4. J. Zhang, Q. Wang, B. Rao, Z. Chen, and K. Hsu, "Swept laser source at 1 ≤m for Fourier domain optical coherence tomography," Appl. Phys. Lett. **89**(7), 073901 (2006).
5. B. Považay, B. Hermann, A. Unterhuber, B. Hofer, H. Sattmann, F. Zeiler, J. E. Morgan, C. Falkner-Radler, C. Glittenberg, S. Blinder, and W. Drexler, "Three-dimensional optical coherence tomography at 1050 nm versus 800 nm in retinal pathologies: enhanced performance and choroidal penetration in cataract patients," J. Biomed. Opt. **12**(4), 041211 (2007).
6. Y. Yasuno, Y. Hong, S. Makita, M. Yamanari, M. Akiba, M. Miura, and T. Yatagai, "In vivo high-contrast imaging of deep posterior eye by 1-um swept source optical coherence tomography and scattering optical coherence angiography," Opt. Express **15**(10), 6121–6139 (2007).

#116884 - $15.00 USD Received 8 Sep 2009; revised 19 Nov 2009; accepted 14 Dec 2009; published 18 Dec 2009

7. R. Huber, D. C. Adler, V. J. Srinivasan, and J. G. Fujimoto, "Fourier domain mode locking at 1050 nm for ultra-high-speed optical coherence tomography of the human retina at 236,000 axial scans per second," Opt. Lett. **32**(14), 2049–2051 (2007).
8. P. Puvanathasan, P. Forbes, Z. Ren, D. Malchow, S. Boyd, and K. Bizheva, "High-speed, high-resolution Fourier-domain optical coherence tomography system for retinal imaging in the 1060 nm wavelength region," Opt. Lett. **33**(21), 2479–2481 (2008).
9. B. Považay, B. Hofer, C. Torti, B. M. Hermann, A. R. Tumlinson, M. Esmaeelpour, C. A. Egan, A. C. Bird, and W. Drexler, "Impact of enhanced resolution, speed and penetration on three-dimensional retinal optical coherence tomography," Opt. Express **17**(5), 4134–4150 (2009).
10. V. J. Srinivasan, D. C. Adler, Y. Chen, I. Gorczynska, R. Huber, J. S. Duker, J. S. Schuman, and J. G. Fujimoto, "Ultrahigh-speed optical coherence tomography for three-dimensional and en face imaging of the retina and optic nerve head," Invest. Ophthalmol. Vis. Sci. **49**(11), 5103–5110 (2008).
11. D. M. de Bruin, D. L. Burnes, J. Loewenstein, Y. Chen, S. Chang, T. C. Chen, D. D. Esmaili, and J. F. de Boer, "In vivo three-dimensional imaging of neovascular age-related macular degeneration using optical frequency domain imaging at 1050 nm," Invest. Ophthalmol. Vis. Sci. **49**(10), 4545–4552 (2008).
12. Y. Yasuno, M. Miura, K. Kawana, S. Makita, M. Sato, F. Okamoto, M. Yamanari, T. Iwasaki, T. Yatagai, and T. Oshika, "Visualization of sub-retinal pigment epithelium morphologies of exudative macular diseases by high-penetration optical coherence tomography," Invest. Ophthalmol. Vis. Sci. **50**(1), 405–413 (2008).
13. Y. L. Chen, D. L. Burnes, M. de Bruin, M. Mujat, and J. F. de Boer, "Three-dimensional pointwise comparison of human retinal optical property at 845 and 1060 nm using optical frequency domain imaging," J. Biomed. Opt. **14**(2), 024016 (2009).
14. K. Bizheva, R. Pflug, B. Hermann, B. Povazay, H. Sattmann, P. Qiu, E. Anger, H. Reitsamer, S. Popov, J. R. Taylor, A. Unterhuber, P. Ahnelt, and W. Drexler, "Optophysiology: depth-resolved probing of retinal physiology with functional ultrahigh-resolution optical coherence tomography," Proc. Natl. Acad. Sci. U.S.A. **103**(13), 5066–5071 (2006).
15. V. J. Srinivasan, M. Wojtkowski, J. G. Fujimoto, and J. S. Duker, "In vivo measurement of retinal physiology with high-speed ultrahigh-resolution optical coherence tomography," Opt. Lett. **31**(15), 2308–2310 (2006).
16. X. C. Yao, A. Yamauchi, B. Perry, and J. S. George, "Rapid optical coherence tomography and recording functional scattering changes from activated frog retina," Appl. Opt. **44**(11), 2019–2023 (2005).
17. J. G. Fujimoto, M. E. Brezinski, G. J. Tearney, S. A. Boppart, B. Bouma, M. R. Hee, J. F. Southern, and E. A. Swanson, "Optical biopsy and imaging using optical coherence tomography," Nat. Med. **1**(9), 970–972 (1995).
18. A. F. Fercher, "Optical coherence tomography," J. Biomed. Opt. **1**(2), 157 (1996).
19. A. F. Fercher, C. K. Hitzenberger, G. Kamp, and S. Y. El-Zaiat, "Measurement of intraocular distances by backscattering spectral interferometry," Opt. Commun. **117**(1-2), 43–48 (1995).
20. G. Häusler, and M. W. Lindner, "Coherence radar' and ``spectral radar' -New tools for dermatological diagnosis," J. Biomed. Opt. **3**(1), 21–31 (1998).
21. S. R. Chinn, E. A. Swanson, and J. G. Fujimoto, "Optical coherence tomography using a frequency-tunable optical source," Opt. Lett. **22**(5), 340–342 (1997).
22. B. Povazay, B. Hermann, V. Kajic, B. Hofer and W. Drexler, "High Speed, Spectrometer Based Optical Coherence Tomography at 1050 nm for Isotropic 3-D OCT Imaging and Visualization of Retinal and Choroidal Vasculature," OSA (BIOMED), paper BMB5 (2008).
23. W. M. Irvine, and J. B. Pollack, "Infrared optical properties of water and ice spheres," Icarus **8**(1-3), 324–360 (1968).
24. G. M. Hale, and M. R. Querry, "Optical constants of water in the 200nm to 200µm wavelength region," Appl. Opt. **12**(3), 555–563 (1973).
25. R. Tripathi, N. Nassif, J. S. Nelson, B. H. Park, and J. F. de Boer, "Spectral shaping for non-Gaussian source spectra in optical coherence tomography," Opt. Lett. **27**(6), 406–408 (2002).
26. A. N. S. Institute, "Safe use of lasers," ANSI Z136.1–2000, American National Standards Institute, (2007).

Introduction

OCT imaging in the 1060 nm wavelength region has recently gained popularity for ophthalmic applications due to the fact that it offers multiple advantages as compared to retinal imaging at shorter wavelengths. Specifically, water, which comprises most of the ocular tissue (cornea, vitreous, lens and retina), has both a local absorption minimum and a dispersion null at ~1060nm, while light scattering from biological tissue decreases monotonically with longer wavelengths. The presence of a local water absorption minimum at 1060nm, combined with the lower scattering tissue coefficient at 1060nm as compared to 800nm, allows for the application of more optical power at the cornea, and effectively at the retinal surface for retinal imaging. The higher optical power, combined with the reduced scattering from melanin in the retinal pigmented epithelium (RPE) at longer wavelengths results in a deeper image penetration and better visualization of the choroidal structure and

#116884 - $15.00 USD Received 8 Sep 2009; revised 19 Nov 2009; accepted 14 Dec 2009; published 18 Dec 2009

vasculature [1–13]. Visualization of choroidal blood vessels and their characterization in terms of number per volume, size and spatial distribution is of particular diagnostic value, since diseases, such as "wet" Age Related Macular Degeneration (AMD) are characterized by choroidal neovascularization, i.e. abnormal growth of new blood vessels. The reduced scattering coefficient of ocular tissue at 1060nm as compared to 800nm has the additional advantage of providing retinal images with significantly better quality in patients with corneal haze or cataracts [9].

Retinal OCT imaging in the 1060 nm wavelength region also has the potential for non-invasive probing of light induced physiological changes in the retina, since retinal photoreceptors are not sensitive to light >900nm [14–16]. Considering the fact that the early stages of retinal diseases are characterized by abnormal function of retinal cells, the ability to image *in-vivo* and non-invasively measure physiological changes in the human and animal retinas and to correlate them with structural abnormalities, can further our understanding of the origins and development of retinal diseases. Such optophysiological recordings have the potential to evolve into a powerful clinical diagnostic and monitoring tool.

Although OCT retinal imaging at 1060nm offers multiple advantages, development of high speed, high axial resolution OCT systems for this wavelength range poses a number of technological challenges. Specifically, axial OCT resolution is primarily determined by the spectral bandwidth of the light source used, while the image acquisition speed is related to the reference mirror velocity (time domain OCT – TD-OCT) [17,18], the data transfer rate of the camera (spectral domain OCT – SD-OCT) [19,20] or the frequency sweep rate of tunable lasers (swept source OCT – SS-OCT) [21]. The first experimental demonstration of the advantages of retinal imaging in the 1060nm wavelength region was accomplished with TD-OCT [1], where porcine retinal samples were imaged *ex-vivo* with axial OCT resolution of 2.8μm in retinal tissue and image acquisition speed of ~0.01 frames/s (2000 A-scans / frame). Later on, improved image penetration into the choroid was demonstrated *in-vivo* in human retina [2] with TD-OCT, with OCT axial resolution of ~7μm in retinal tissue and image acquisition rate of 150 A-scan/s. Recent advances in CCD and tunable laser technology have lead to significant improvement of the image acquisition rate of retinal OCT systems operating in the 1060nm wavelength region, specifically, up to 47 kHz for SD-OCT [8] and up to 236 kHz for SS-OCT [7]. By employing broad bandwidth continuous wave light sources such as superluminescent diodes (SLDs) and amplified spontaneous emission (ASE) sources, with spectral outputs centered in the range of 1020nm–1040nm, axial resolutions of 5.7μm [8] and 7μm [22] were achieved *in-vivo* in human retinas with SD-OCT systems. Currently the trade-off between tunable range and sweep rate of tunable light sources limits the axial resolution of SS-OCT systems in the 1060nm wavelength range to ~10μm in retinal tissue [6].

Until recently, it was generally accepted that the local peak at ~980nm and the fast rise beyond 1120nm in the water absorption profile [23,24] define an optical "window" [see Fig. 1(a)], which limits the effective spectral bandwidth transmitted through the anterior part of the eye to the retinal surface. The full width at half maximum (FWHM) of this optical window is ~100nm, centered at ~1060nm, which effectively limits the OCT axial resolution in human retina to ~3.6μm. This value is a theoretical estimate, since in practice the spectral transmission characteristics of the optical and fiberoptic components of the imaging system, along with the spectral efficiency of the detector can reshape the input optical spectrum and effectively reduce the measured axial OCT resolution. So far this theoretical limit has not been reached experimentally due to technical difficulties. Specifically, CW light sources such as SLDs and ASE sources may provide spectral emission bandwidths of ~100nm or broader, but the spectra of currently commercially available or published research grade CW light sources are centered in the range of 1020nm - 1040nm, away from the center of the water absorption optical window (1060nm). This severely reduces the spectral bandwidth transmitted to the retinal surface. Although the sweep ranges of commercially available tunable lasers are centered almost exactly at 1060nm, currently they are limited to ~50-70nm

#116884 - $15.00 USD Received 8 Sep 2009; revised 19 Nov 2009; accepted 14 Dec 2009; published 18 Dec 2009

at FWHM of the tunable range, corresponding to OCT axial resolution in free space of ~7μm to 10μm. The actual axial OCT resolution in the human retina in this case will be dependent on the spectral reshaping of the imaging beam due to water absorption in the eye.

This study aimed to a) determine if spectral reshaping of the input optical spectrum can overcome at least partially the retinal OCT resolution limitations imposed by the water absorption profile in the 1060nm wavelength range; and b) investigate the practical limits to the highest OCT axial resolution achievable *in-vivo* in human and small animal retinas, by considering spectral reshaping, the ANSI standard power limitations and the OCT system design. For the purpose of this study we have developed a simple computational model and have verified its results experimentally. The outcome of this study could serve as an insight and a guideline to research groups and companies developing CW or tunable light sources for high resolution ophthalmic (retinal) SD-OCT and SS-OCT systems operating in the 1060nm wavelength range.

Methods

Computational model

We have developed a simple computational model, which considers the effect of water absorption on the spectral bandwidth and central wavelength of an optical beam propagating through a water layer that approximates the water content of the rodent and human eye. A schematic representation of the model is shown in Fig. 1. An optical imaging beam with initial spectral content and intensity $I_0(\lambda)$ is incident on an eye [Fig. 1(b)] with physical length d (distance between the front surfaces of the cornea and the retina), or a water cell with the same physical thickness, d. The model assumes that wavelength dependent scattering in the eye is negligible as compared to water absorption, which is true for the vitreous at ~1060nm.

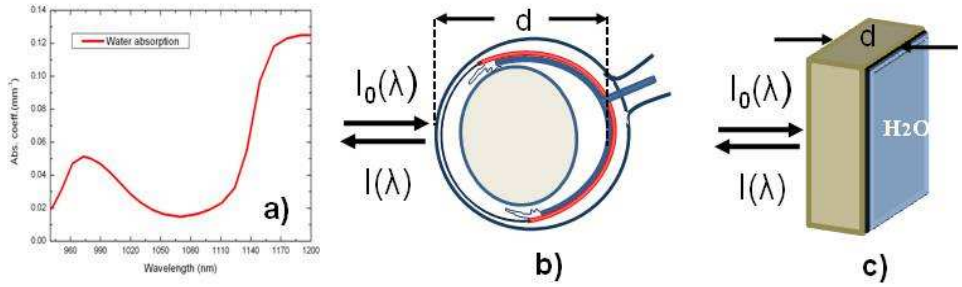

Fig. 1. Water absorption profile (a); Schematic representation of the eye (b) and a water cell (c): $I_0(\lambda)$ – intensity of the incident optical beam; $I(\lambda)$ – intensity of the back-reflected optical beam; d – physical distance between the cornea and retina (b), equivalent to the thickness of the water cell (c).

The intensity and spectral content of the optical beam back-reflected from the retina [Fig. 1(b)] or the back side of the water cell [Fig. 1(c)] and measured after double pass though the eye / water cell is $I(\lambda)$. For weekly absorbing media such as water, the relationship between the intensity of the incident and detected optical beams is given by Beer-Lambert law:

$$I(\lambda) = I(\lambda_o)\exp\left(-2\mu_a(\lambda)d\right) \quad (1)$$

Here $\mu_a(\lambda)$ is the wavelength dependent water absorption coefficient [Fig. 1(a)] and the factor of 2 in the exponent accounts for the double pass of the optical beam through the eye / water cell. For our model we used published values for water absorption [23,24] and assumed that the average lengths of the rodent and human eye are 5mm and 25mm respectively.

#116884 - $15.00 USD Received 8 Sep 2009; revised 19 Nov 2009; accepted 14 Dec 2009; published 18 Dec 2009

Experimental verification

For the experimental verification of the model, we modified the spectral output of a commercially available light source (Superlum Inc., $\lambda c = 1020$ nm, $\Delta\lambda = 110$ nm and $P_{out} = 10$ mW) and interfaced it to a compact, fiber-based SD-OCT system designed to operate in the 900-1200nm wavelength range. Figure 2 shows a schematic of the SD-OCT system:

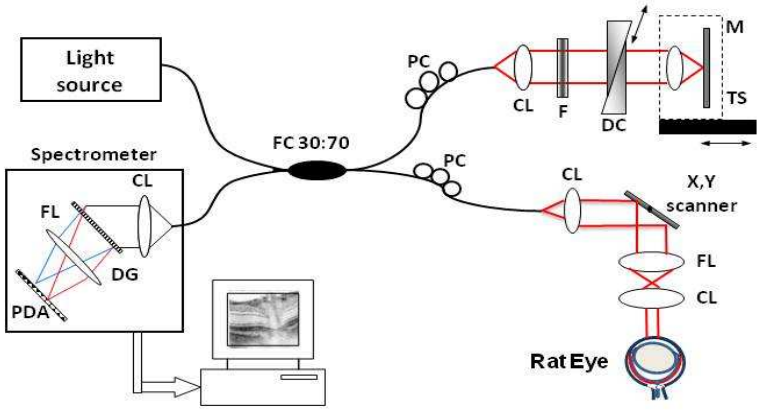

Fig. 2. Schematic of the ultrahigh-resolution SD-OCT system: (CL) - collimating lenses, (DC) - dispersion compensation unit, (NDF) - neutral-density filters, (M) – mirror, (PC) - polarization controllers, and (TS) - translation stage. The spectrometer consists of a collimating lens (CL), a volumetric diffraction grating (DG), a focusing lens (FL) and a high speed InGaAs CCD camera.

All optical and fiber optic (Corning 1060-HP) components of the FD-OCT system were selected to support the propagation of broadband light through the systems with minimal spectral and power losses.The interference signal is detected by a high efficiency custom-built spectrometer (P&P Optica Inc.), which utilizes a fast, 1024 pixel linear array CCD camera (SUI Goodrich) with 47 kHz readout rate. The spectrometer is designed for the spectral range 940 - 1120nm and provides average absolute grating efficiency >80% over the entire spectral range, and spectral resolution of $\delta\lambda = 0.15$nm. Data is acquired with a framegrabber (NI) and is processed and displayed by a computer. More detailed description of the system design and test performance can be found in ref [8]. The effect of the water content of the the human and rodent eyes was simulated by inserting identical water cells with appropriate lengths in the sample and reference arms of the SD-OCT system.

Results and discussion

Computational results

Figure 3 shows the spectral shape, bandwidth and power losses for an input spectrum of Gaussian shape, centered at 1060nm with a spectral bandwidth of 200nm as propagating through water cells with thickness equivalent to the legth of the human or rodent eye. Figure 3(a) shows an overlay of the input spectrum (black line) and the water absorption profile (grey line). Comparison of the overall shape and power losses resulting from double pass propagation of the imput beam through 5mm (blue line) and 25mm (red line) water layers is shown in Fig. 3(b). Total power loss of 80% and 46% was computed for the case of 25mm and 5mm thick water layers respectively, by integrating over the spectral densities below the curves in Fig. 3(b).

#116884 - $15.00 USD Received 8 Sep 2009; revised 19 Nov 2009; accepted 14 Dec 2009; published 18 Dec 2009

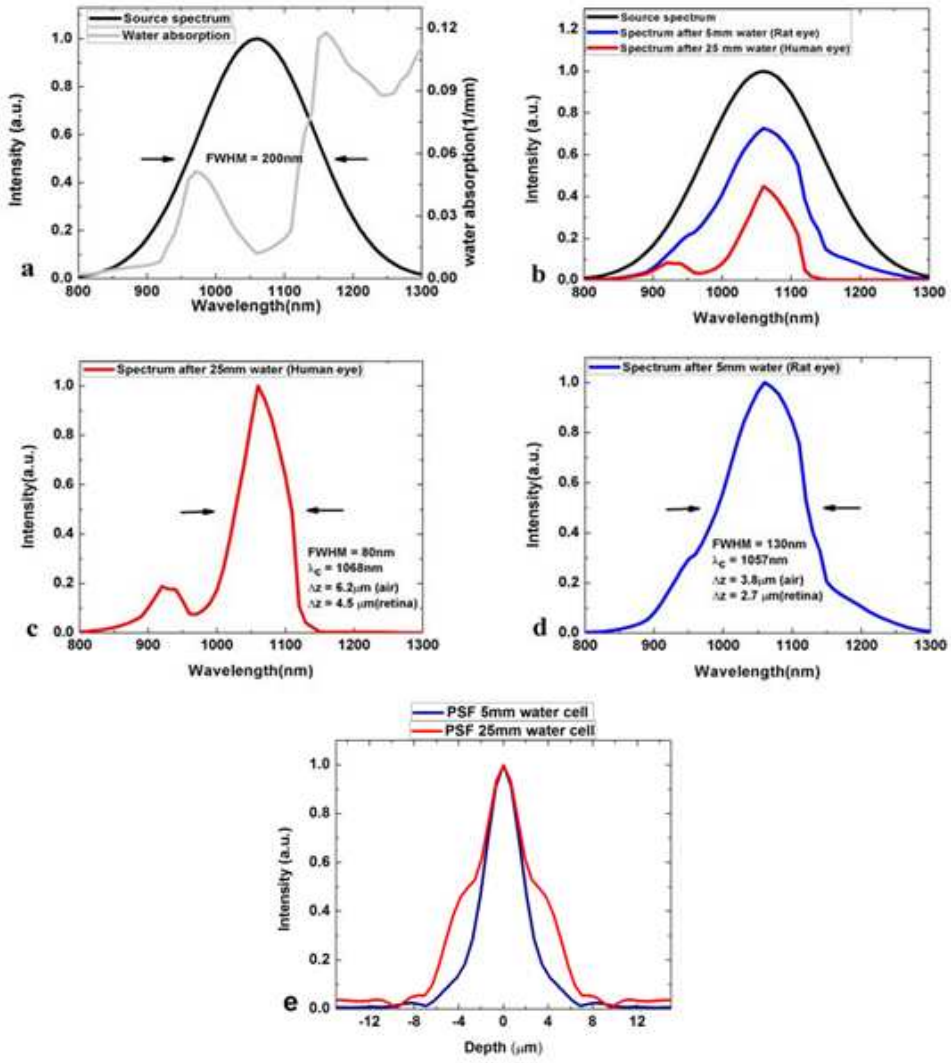

Fig. 3. Graphical representation of the spectral shape, bandwidth and power losses due to water absortion, calcualted for a double pass of the imaging beam (blak line) thourgh water layers of 5mm (blue line) and 25mm (red line), corresponding to average lengths of a human and rat eye respectively. (a) Gaussian shaped input spectrum with 200nm spectral bandwidth, centered at 1060nm and the water absorption profile (grey line). (b) Comparative spectral power losses. Spectral shape and bandwidth changes, and theoretical values for the corresponidng OCT axial resolution in the retina for the case of 25mm (c) and 5mm (d) thisck water layers. Comparison of the PSFs (e) computed by Fourier transforming the the spectra shown in (c) and (d).

Figure 3(c) shows that water absorption in a human eye of 25mm average length limits the maximum useful spectral bandwidth of the imaging beam to ~80nm, corresponding to OCT axial resolution of ~4.5µm in the retina. In the case of the much smaller rodent eye, the useful imaging bandwidth is reduced to ~130nm [Fig. 3(d)], corresponding to axial OCTresolution of ~2.7µm in the rat retina. The spectra shown in Fig. 3(c) and 3(d) were Fourier transformed to detrmine the effect of the non-Gaussian shape of the water affected spectra on the resulting PSFs [Fig. 3(e)].

Achieving axial OCT resolution < 3µm in the human retina at ~1060nm, comparable to the highest resolution demonstrated previously with research grade OCT systems operating at ~800nm, may be possible by expanding the usable spectral bandwidth around 1060nm by

#116884 - $15.00 USD Received 8 Sep 2009; revised 19 Nov 2009; accepted 14 Dec 2009; published 18 Dec 2009

reshaping the spectrum of the incident imaging beam. Numerical specral reshaping has been used in the past to suppress the appearance of sidelobes in the OCT PSF [25]. To test the idea of spectral reshaping, the example input spectrum [Fig. 3(a), black line] was multiplied with an inverse function of the water absorption [Fig. 3(a), grey line] to generate reshaped input spectra for the two cases of 25mm water layer [Fig. 4(a), black line] and 5mm water layer [Fig. 4(b), black line]. By applying the re-shaped input spectra to the computational model described above, axial resolution of 1.8μm, corresponding to spectral bandwidth of 200nm centered at 1060nm, can be achieved theoretically in the human or rat retina.

The computational results shown in Fig. 4(a) and 4(b), also demonstrate the major difficulty with achieving the theoretical resolution in practice. Due to the sharp increase of water absoption (grey line) for wavelengths longer than 1120nm, more than 80% of the input power of the reshaped spectrum for the human eye [25mm water layer, Fig. 4(a)] is contained in a fairly narrow spectral range (1150nm – 1200nm), corresponding to the tail of the Gaussian shaped detected spectrum. Since in the case of OCT imaging of the human retina at ~1060nm, the safety guidelines of the ANSI standard [26] limit the spectral power incident on the cornea to ~2mW for 10s exposure, the power remaining for imaging is not sufficient for obtaing high contrast images of the retina and for imaging choroidal blood vasculature. In the case of the rodent eye, the power losses attributed to water absorption are significantly smaller, therefore achieving axial OCT resolution of 2μm or better in the rat retina is limited by the availability of light sources with spectra close to the theoretical one shown in Fig. 4(b) and the design of the OCT system, capable of sustaining that spectrum. One way to achieve improvement in the axial OCT resolution in the human retina within the power guidelines of the ANSI standard, is to truncate the long wavelength end of the Gaussian input spectrum used in the computational model [Fig. 4(c)]. In this case the spectral bandwidth is limited to ~160nm and the cetral wavelength is shifted to 1040nm, which results in theoretical limit of ~2μm for the axial OCT resolution in the human retina. The corresponding reshaped spectrum is shown in Fig. 4(d).

#116884 - $15.00 USD Received 8 Sep 2009; revised 19 Nov 2009; accepted 14 Dec 2009; published 18 Dec 2009

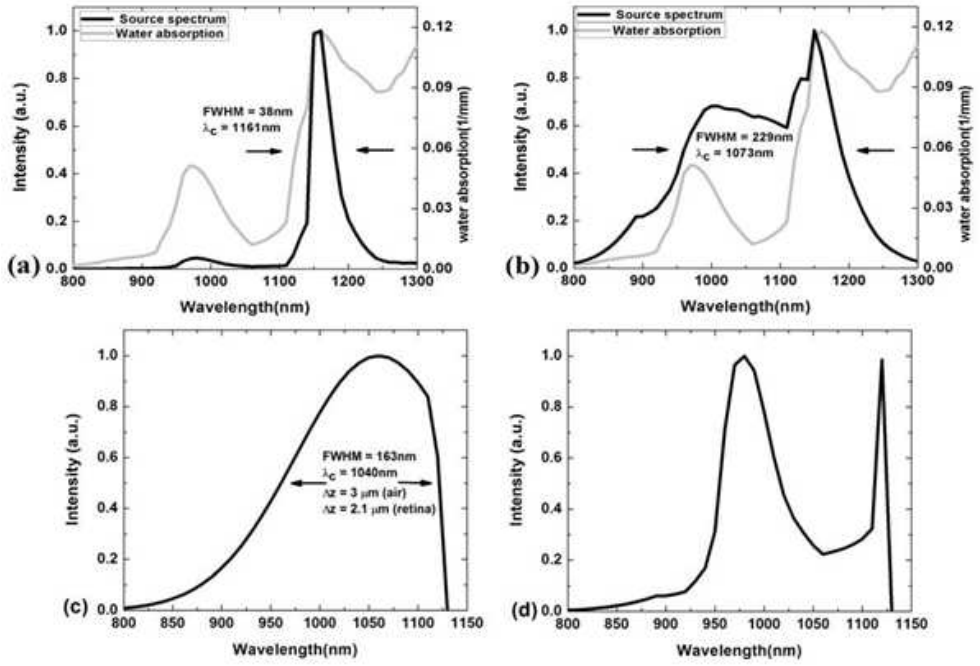

Fig. 4. Reshaped input imaging spectra for the (a) 25mm (human, black line) and (b) 5mm (rat, black line) thick water layers described in the computational model. The reshaped spectra were generated by multiplying the original Gaussian input spectrum from Fig. 3(a) with an inverse function of the water absorption [Fig. 1(a)]. The figure shows the major limitation (power loss) to achieving the theoretical axial OCT resolution of 1.8μm in the human retina. Truncated Gaussian spectrum (c) and the corresponding reshaped input spectrum for the human eye (d).

Experimental results

To demonstrate experimentally that spectral re-shaping of the incident imaging beam can lead to improvement in the OCT axial resolution for retinal imaging at ~1060nm, we modified the spectral output of a commercially available SLD based light source (Superlum Inc.) to increase the spectral power at ~980nm where water absorption has a local maximum. The original light source was comprised of two SLDs with partially overlapping spectra and power outputs selected to result in a nearly Gaussian shaped spectrum of the light source [Fig. 5(a), black line]. We modified the original SLD with assistance from Superlum to increase the power output of the shorter wavelength SLD, which was centered at ~980nm, overlapping with the water absorption peak. The spectral shape of the modified light source is shown in Fig. 5(a) (red line), and the total power output of the source was ~12mW. Note that the spectra shown in Fig. 5(a) are the spectra of the original and modified light sources measured at the detection end of the SD-OCT system with a silver mirror used as a sample in the imaging arm of the system. Therefore, this measurement automatically accounts for any spectral losses related to the transmission bandwidth of all optical and fiber optic components in the SD-OCT system, as well as the spectral sensitivity of the CCD camera. The graphs in black and red colors in Fig. 5(b) and Fig. 5(c) show the spectra measured at the detection end of the SD-OCT system with the original and modified light sources, for water cells of 5mm and 25mm thickness respectively, inserted in the sample arm of the OCT system before the mirror. Figure 5(d) and 5(e) show the measured axial PSFs of the SD-OCT system for the spectra shown in Fig. 5(b) and Fig. 5(c). In the case of the 5mm water cell, 4.2μm axial resolution was measured in air with the sample mirror, which corresponds to 3μm axial resolution in the rat retina assuming an average refractive index of 1.38 for retinal tissue in the

#116884 - $15.00 USD Received 8 Sep 2009; revised 19 Nov 2009; accepted 14 Dec 2009; published 18 Dec 2009

1060nm wavelength range. This constitutes about 30% improvement of the axial OCT resolution in the rat eye as compared to the one achieved with non-reshaped spectrum of the standard, commercially

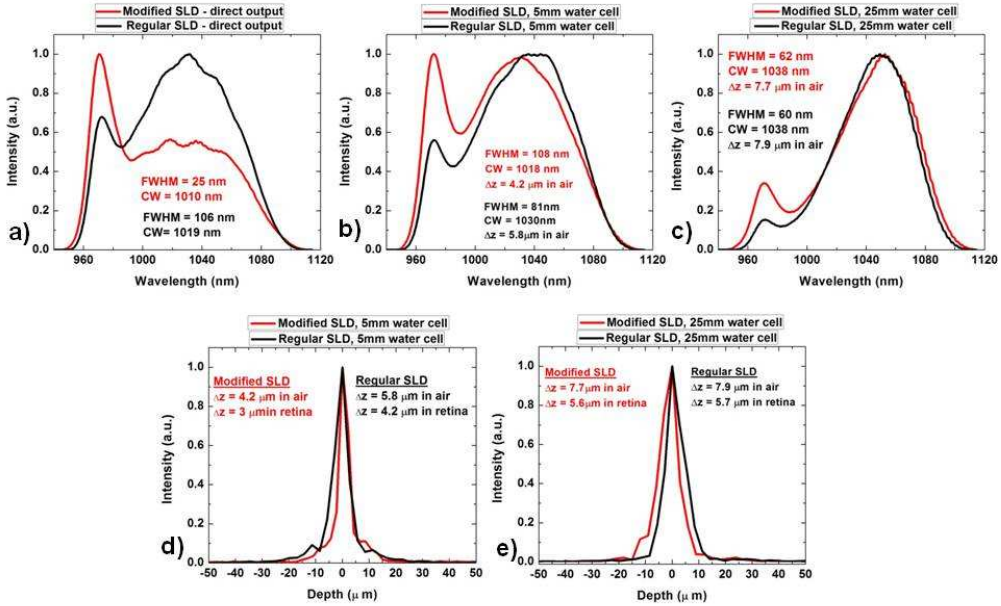

Fig. 5. Spectra of the original and modified SLD based light sources measured at the detection end of the SD-OCT system from a mirror reflection in the sample arm (a). Spectra of the original and modified SLD based light sources measured after a double pass of the imaging beam through a 5mm (b) and 25mm thick (c) water cells, inserted in the sample arm of the system. PSFs measured with the SD-OCT system with the two light sources and with 5mm (d) and 25mm (e) water cells in both arms of the imaging system.

available light source [8]. In the case of the 25mm water cell, the measured resolution from the mirror reflection was ~7.8μm, corresponding to ~5.7μm imaging resolution in the human retina, assuming an average refractive index of 1.38 of retinal tissue. In this case, spectral re-shaping of the SLD based light source was not sufficient to result in significant enough improvement of the axial OCT resolution as compared to previously published results [8].

To demonstrate experimentally the effect of the high axial OCT resolution on the image quality, OCT tomograms were acquired *in-vivo* from the retinas of Long Evans rats. The animals were anesthetized by intra-peritoneal injection of ketamine (80mg/kg) and xylazine (8mg/kg). Subsequent pupil dilation was achieved by administering 1-2 drops of tropicamide (Mydriacyl, 1%) per eye. All animal experiments were conducted in accordance with animal protocols approved by the Animal Ethics Review Boards of the University of Waterloo and St. Michael's Hospital, Toronto. The eye imaging probe was designed to project a parallel beam of 2.5mm diamter onto the rat's pupil, resulting in lateral resolution better than 5μm in the rat retina. To achive optimum coupling of the optical beam into the rat eye, the animals were placed on a stage that allowed angualr adjustment of the rat eye with respect to the direction of the imaging beam.

Figure 6 shows representative 2D and 3D images of healthy rat retinas acquired *in-vivo*. The images were acquired at 47kHz with 1.5mW power of the optical beam incident on the rat cornea and 101dB sensitivity. The image size is 1000 A-scans x 220 pixels. The image in

#116884 - $15.00 USD Received 8 Sep 2009; revised 19 Nov 2009; accepted 14 Dec 2009; published 18 Dec 2009

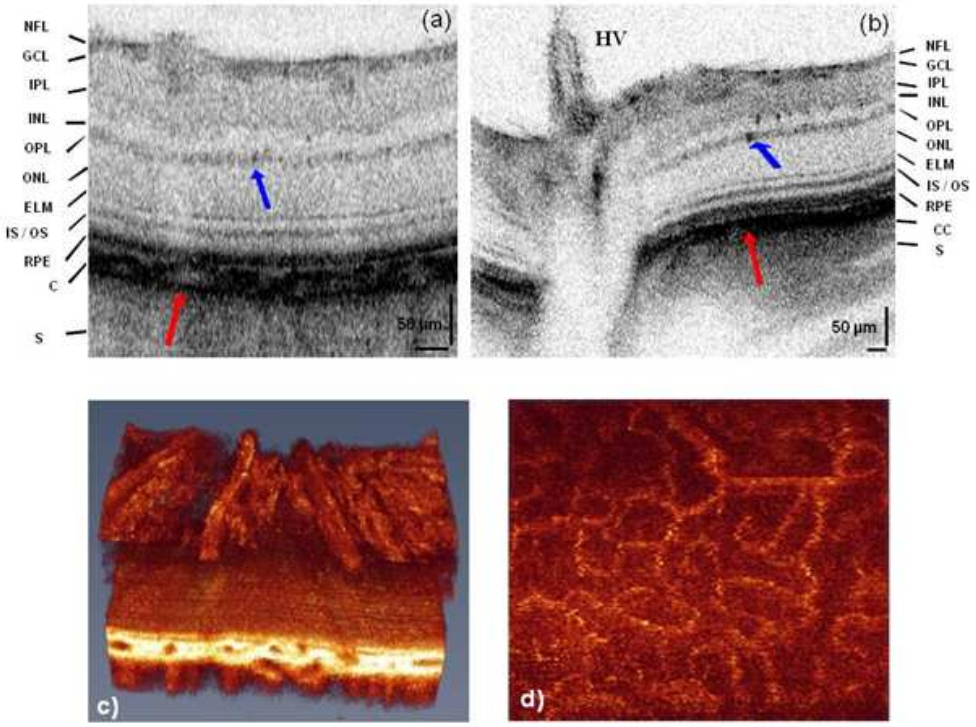

Fig. 6. Two-dimensional images of rat retina acquired *in-vivo* away from the optic disc (a); and at the optic disc (b). Image dimensions are 1000 x 220 pixels. Both images show clear visualization of all retinal layers, as well as the cross-sections of multiple choroidal vessels marker with red arrows. Cross-sections of capillaries located at the inner plexiform (IPL) and outer plexiform (OPL) layers are distinctly visible on both images and marked with blue arrows. Red arrows point at choroidal blood vessels. Figure 6(b) shows the remains of the hyaloids vessel (HV). Figure 6(c) shows a representative 3D stack of 172 B-scans of the rat retina. Figure 6(d) shows an en-face cross-section of the retina obtained from the 3D stack at the location of the outer plexiform layer of the retina. The en-face image shows the intricate network of capillaries, that correspond to the highly reflective black spots in observed in the 2D retinal images (blue arrows).

Figure 6(a) was acquired away from the optic disc and shows clear visualization of all intra-retinal layers, cross-sections of blood vessels in the underlying choroid and part of the sclera. The image in Fig. 6(b) was acquired from the area around the optic disc and shows a cross-section of the remains of the hyaloid blood vessel (HV). The small black circular features observed in the inner- and outer plexiform layers of the rat retina in both images correspond most likely to reflections from red blood cells in the tiny (~10 µm diameter) capilaries. Resolving of such small morphological details in the retina is fascilitated by the improved axial OCT resolution.

Other morphological details of the rat retina are better observed in the 3D movies shown in Fig. 7. The movies were generated from 3D stacks of B-scans acquired away [Fig. 7(a)] and in the vicinity of the optic disk [Fig. 7(b)]. The 3D stacks in the movies are composed of 172 and 256 frames respectively.

#116884 - $15.00 USD Received 8 Sep 2009; revised 19 Nov 2009; accepted 14 Dec 2009; published 18 Dec 2009

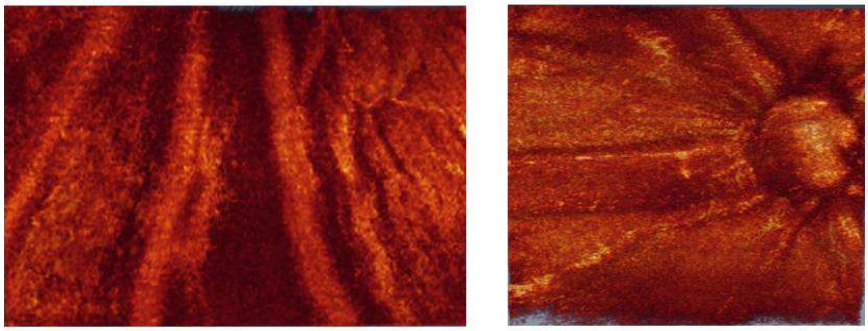

Fig. 7. Single-frame excerpts from 3D movies of living rat retina acquired a) away from the optical disc (Media 1); and b) at the optical disc (Media 2). Image dimensions are 1000 x 250 pixels, 172 frames (a); 256 frames (b).

To determine the effect of the improved axial OCT resolution on the image quality, OCT tomograms were acquired with the original and the modified light source at approximately the same location in the rat retina of the same animal. Representative images are shown in Fig. 8.

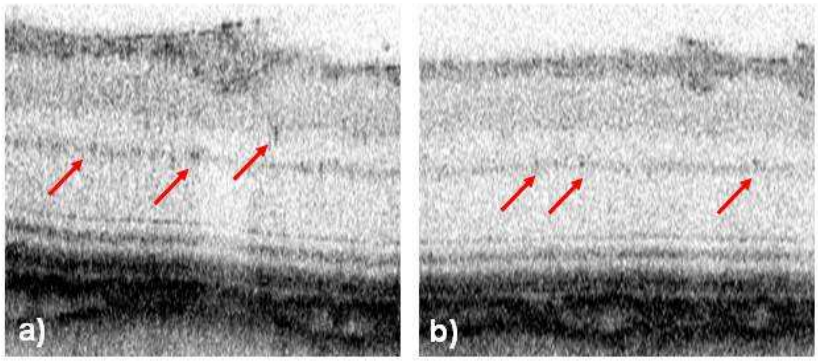

Fig. 8. Comparison of retinal OCT tomograms acquired with the original (a) and the modified (b) SLD based light source. The image acquired with the modified light source shows slightly better visualization of the boundaries of the inner retinal layers, as well as better definition of the reflections from retinal capillaries (red arrows).

Visual comparison of the two images shows that the one acquired with the modified light source [Fig. 8(b)] offers slightly better delineation of the retinal layer boundaries, and improved definition of the highly reflective spots that correspond to reflections from retinal capillaries (red arrows). Since the experimental improvement of the axial OCT resolution in our case was limited to only ~30% due to technical difficulties of building a light source with spectral output close to the one suggested by the theoretical model, and given the size of morphological features in the rat retina, dramatic changes in the image quality of the retinal tomograms were not expected. However, future development of light sources based on the model presented here, could potentially generate 2µm axial OCT resolution in the rat retina, which will constitute of factor of 2 resolution improvement as compared to recently published results [8]. If the lateral imaging resolution is also improved by combing OCT with an adaptive optics (AO) system, diffraction limited, isotropic imaging resolution of ~2µm can be achieved in the rat retina that would allow for observation of individual photoreceptors in 3D.

Discussion

Results from the computational model [Fig. 3(c)] show that the use of a Gaussian shaped spectrum in the imaging beam of an SD-OCT system designed for retinal imaging at 1060nm,

#116884 - $15.00 USD Received 8 Sep 2009; revised 19 Nov 2009; accepted 14 Dec 2009; published 18 Dec 2009

and the water absorption profile in this wavelength range ultimately limit the maximum achievable axial OCT resolution to ~4.5µm in the human retina. Theoretically, reshaping of the OCT incident on the human cornea can improve the axial OCT resolution in human retina by a factor of ~2 [Fig. 4(c) and 4(d)]. However the extent of the reshaping is limited by the maximum permissible exposure limit defined by the ANSI standard [26]. For the spectral range 900nm – 1200nm, 7mm limiting aperture and 10s exposure, the ANSI limit for the power incident on the human cornea is ~2mW. Previous studies [8] conducted with a commercially available SLD based light source (same as the basic SLD unit used in the current study before the modification) have shown that 5.7µm axial OCT resolution can be achieved in the human retina with imaging power of < 1mW at the cornea. A reshaped spectrum similar to the one presented in Fig. 4(d) could theoretically result in ~2µm axial OCT resolution in the human retina. However, our calculations show that the total optical power corresponding to this reshaped spectrum will be ~3mW, which is higher that ANSI limit for 10s exposure. Further truncation of the shorter wavelength end of the reshaped spectrum [Fig. 4(d)], or partial magnitude reduction of the peak at ~980nm could bring the imaging power incident on the cornea, below the ANSI maximum permissible exposure at the expense of lower axial OCT resolution in the human retina (~3.5µm). Such a trade-off would be very advantageous, since it would constitute at least a factor of 2 improvement over previously published [5–15] axial OCT resolution in the human retina in the 1060nm wavelength range. Furthermore, it will bring the axial resolution of 1060nm Ophthalmic OCT systems closer to the resolution (~2.5µm) achieved in human retina with OCT systems operating in the 800nm wavelength range.

In the case of imaging the rat retina, use of spectral reshaping offers theoretically and experimentally, significant improvement as compared to previous studies conducted with a commercially available SLD [8]. In this study, the allowed modifications to the SLD unit limited the imaging power incident on the rat cornea to 1.5mW and the spectral modifications only to the shorter wavelength end of the SLD spectrum. With these spectral modifications we achieved ~30% improvement of the axial OCT resolution in the rat retina. Future development of light sources with properly shaped emission spectra could potentially allow the achievement of ~2µm axial OCT resolution in the rodent retina, close to the theoretical limit predicted in this study [Fig. 4(b)]. The high axial OCT resolution can improve the visibility of small features in the rodent retina, for example the small capillaries in the plexiform layers, as well as the sharpness of the retinal layer boundaries in the OCT images. The last feature is directly related to the precision and optimal performance of layer segmentation algorithms and the accurate thickness measurement of individual retinal layers, which can serve as a biomarker of developing retinal diseases. Furthermore, if the SD-OCT system is combined with an adaptive optics (AO) system, isotropic imaging resolution of ~2µm can be achieved in the rodent retina due to the shorter focal length of the animal eyes. Such imaging resolution could potentially allow visualization of individual photoreceptors in 3D, which would be of significant interest to clinical ophthalmologists studying neurodegenerative diseases.

The strong attenuation of the optical imaging power in the human eye resulting from water absorption in the vitreous and the anterior chamber will also have a detrimental effect on the contrast and image penetration depth of retinal OCT tomograms. Assuming an average water absorption coefficient of $0.04mm^{-1}$ for the spectral range of 950nm – 1130nm, a double pass of the optical beam through a human eye of 25mm average length, would result in ~9dB loss of SNR. Considering the fact that current research grade SD-OCT and SS-OCT systems [5–15] provide SNR of 95dB to 100dB for imaging power of ~1mW, such a loss could affect significantly the OCT image penetration depth into the choroid.

In the case of small animal eye (for example rodents) imaging, the SNR loss due to water absorption will be in the order of 2dB, which should not affect significantly the contrast or

#116884 - $15.00 USD Received 8 Sep 2009; revised 19 Nov 2009; accepted 14 Dec 2009; published 18 Dec 2009

image penetration depth of the 1060nm OCT retinal tomograms. This is clearly demonstrated by the rat retina images acquired with modified light source.

The simple computational model described in this manuscript can serve as a guideline for future design of novel light sources, targeting to improve the axial OCT resolution of ophthalmic OCT systems, designed for imaging the human or animal retina in the 1060nm wavelength range. Although the model was tested experimentally with a SD-OCT system, improvement of the axial OCT resolution in retinal imaging through spectral reshaping is feasible both in TD-OCT and SS-OCT. It is important to note that other factors such as the spectral efficiency of the detector (whether it is a single photodiode, a dual balanced detector or a linear array CCD), as well as the spectral characteristics of all optical and fiber optic components in the imaging system will further modify the emission spectrum of the light source, as it propagates through the system. These modifications can have positive or negative effect on axial OCT resolution. Furthermore, extending the spectrum of the input imaging beam to < 900nm can result in multimodal light propagation through the fiber based OCT system, which can have a detrimental effect on the OCT axial resolution and SNR In the OCT system used for the experimental verification of the computer model, we used fibers with cut-off wavelength of 905nm and the shorter wavelength end of the spectrum of the modified SLD light source was located at ~950nm. If the exact spectral characteristics of some of the OCT system components are know apriori, they can be included in the computer model for better guidance of the final design of the desired light source spectrum. In our case, we have included the spectral efficiency of the InGaAs CCD camera in our computational model. Other factors, for example the spectral transmission of fiber couplers or fiberoptic isolators are polarization dependent, therefore, their influence on the final detected spectrum can only be approximated in the proposed computer model.

Conclusions

Improving the axial resolution of ophthalmic OCT systems designed for retinal imaging in the 1060nm wavelength range is a key factor to visualization of small morphological details in the human or animal retina that can be associated with diagnostic or therapeutic markers of many retinal diseases. Furthermore, high axial OCT resolution can improve the precision of segmentation algorithms designed for thickness measurement of individual retinal layers. In this manuscript we have proposed and tested the effectiveness of spectral shaping as a method for improving the axial resolution in the retina of OCT systems designed for the 1060nm wavelength region. The results from this study not only establish the theoretical and practical limits to the highest axial OCT resolution achievable at 1060nm, but also can serve as a guideline for development of novel light sources for UHROCT at 1060nm.

Acknowledgments

The authors are very grateful for the inkind support provided by Superlum Inc, in particular, V. Shidlovski. We also would like to thank M. Xia, H. Van der Heide and J. Szubra for their assistance with the electronic and mechanical designs, and X. Zhao from St. Michael's Hospital, Toronto for assistance with the animal preparation. This work was supported in part by NSERC, CIHR doctoral fellowship, Ortho-Biotec (Canada) and Ontario Centers of Excellence grants and the Walter Family fund (St Michael's Hospital).

#116884 - $15.00 USD Received 8 Sep 2009; revised 19 Nov 2009; accepted 14 Dec 2009; published 18 Dec 2009